A Wnt/β-catenin signaling driven adipocyte population required for beiging and glucose homeostasis

Zhi Liu,[1,2,4] Tian Chen,[1,2,4] Sicheng Zhang,[1,2] Tianfang Yang,[1] Yun Gong,[3] Hong-Wen Deng,[3] Ding Bai,[2] Weidong Tian,[2*] and YiPing Chen[1,5,*]

[1]Department of Cell and Molecular Biology, Tulane University, New Orleans, LA, USA

[2]State Key Laboratory of Oral Diseases, National Clinical Research Center for Oral Disease, West China Hospital of Stomatology, Sichuan University, Chengdu, Sichuan Province, China

[3]Tulane Center of Biomedical Informatics and Genomic, Deming Department of Medicine, School of Medicine, Tulane University, New Orleans, LA, USA

[4]These authors contributed equally

[5]Lead contact

[*]Correspondence: drtwd@sina.com (W.T.), ychen@tulane.edu (Y.C.)

ABSTRACT

Wnt/β-catenin signaling has been well established as a potent inhibitor of adipogenesis. Here, we identified a population of Wnt/β-catenin signaling driven adipocytes in embryonic and adult mouse fat depots. We showed that Wnt/β-catenin signaling activation in these cells relies on AKT/mTOR signaling intracellularly and is essential for cell survival. Such adipocytes are distinct from classical ones in transcriptomic and genomic signatures and can be induced from various sources of mesenchymal stromal cells including human cells. Using genetic lineage-tracing and targeted cell ablation mouse models, these adipocytes were shown to not only convert into beige adipocytes directly but be also required for beige fat recruitment under thermal challenge, demonstrating a central role in initiating adaptive thermogenesis. Mice bearing targeted ablation of these adipocytes exhibited glucose intolerance, while mice receiving exogenously supplied such cells manifested enhanced glucose utilization. Our studies uncover a unique adipocyte population in regulating beiging and systemic glucose homeostasis.

KEYWORDS

Adipocytes, β-catenin signaling, AKT/mTOR signaling, beiging, glucose homeostasis

INTRODUCTION

Adipose tissues, consisting of white adipose tissue (WAT) and brown adipose tissue (BAT), play a critical role in maintaining whole-body metabolic homeostasis, with WAT serving for energy storage and BAT for energy dissipation to produce heat (Cannon and Nedergaard, 2004; Rosen and Spiegelman, 2014). In addition to white and brown fat cells that are differentiated from heterogenous stromal vascular fractions (SVFs) of distinct lineages (Hepler et al., 2017; Rosenwald and Wolfrum, 2014; Schwalie et al., 2018), a third type of inducible adipocyte exists known as beige or brite adipocytes that are transiently generated in WAT depots in response to external stimulations such as environmental cold acclimation (Bostrom et al., 2012; Ikeda et al., 2018; Wu et al., 2012). Like brown adipocytes, activated beige adipocytes through "beiging" or "browning" process of WAT express key thermogenic marker uncoupling protein 1 (UCP1) and exert adaptive thermogenic function (Ishibashi and Seale, 2010; Petrovic et al., 2010). Despite that the capacity for thermogenic fat cells (i.e., brown and beige adipocytes) to protect against diet-induced obesity and metabolic disorders has been recognized (Bartelt and Heeren, 2014; Crane et al., 2015; Hasegawa et al., 2018; Ikeda et al., 2017; Lowell et al., 1993; Tseng et al., 2010), a comprehensive understanding of developmental origins and regulatory mechanism of beiging is still missing, partially due to the cell-type complexity in adipose tissues. It has been appreciated that beige adipocytes arise by both de novo adipogenesis from progenitor cells and direct conversion/transdifferentiation from white adipocytes (Barbatelli et al., 2010; Shao et al., 2019; Wang et al., 2013). While previous profiling studies have identified some specific markers (for example, CD137 and CD81) for progenitors of beige adipocytes (Oguri et al., 2020; Wu et al., 2012), the cellular origin of beige adipocytes derived from direct conversion remained elusive.

Wnt/β-catenin (canonical) signaling pathway plays a fundamental role in cell proliferation, differentiation, and tissue homeostasis. In the presence of Wnts, "destruction complex" including glycogen synthase kinase 3 (GSK-3) is inhibited and cytoplasmic β-catenin translocates into the nucleus and interacts with TCF/LEF transcription factors to activate downstream target genes (Cadigan and Liu, 2006; Dale, 1998). In addition, β-catenin nuclear translocation can also be triggered by other intracellular factors such as AKT and $G\alpha_s$, leading to the activation of Wnt/β-catenin signaling in a ligand- and receptor-independent manner (Fang et al., 2007; Regard et al., 2011). Despite the consensus that Wnt/β-catenin signaling imposes negative effects on adipogenesis by inhibiting Pparγ (Longo et al., 2004; Ross et al., 2000; Waki et al., 2007), clues have been pointing to potentially crucial roles of Wnt/β-catenin signaling in adipogenesis and adipose tissue function. For instance, β-catenin and Tcf7l2, two key effectors of canonical Wnt signaling pathway, are expressed by mature adipocytes. Genetic mutations in *Ctnnb1* (encoding β-catenin) and *Tcf7l2* lead to impaired adipocyte development and maturation (Chen et al., 2020; Chen et al., 2018). Particularly, loss of *Tcf7l2* in mature adipocytes gives rise to adipocyte hypertrophy, inflammation, as well as systemic glucose intolerance and insulin resistance, implying an important biological role for Wnt/β-catenin signaling in adipose function (Chen et al., 2018; Geoghegan et al., 2019). However, direct evidence is lacking.

RESULTS

A Unique Fraction of Murine Adipocytes Displays Wnt/β-catenin Signaling Activity

In a survey for the presence of active Wnt/β-catenin signaling in any developing and mature adipocytes, we used the Wnt/β-catenin signaling specific reporter mouse line *TCF/Lef:H2B-GFP* (hereafter *T/L-GFP*) that allows for real-time monitoring of Wnt/β-catenin activity at single-cell resolution (Ferrer-Vaquer et al., 2010). Surprisingly, we virtually observed a

subset of Perilipin$^+$ adipocytes that exhibited Wnt/β-catenin signaling activity interspersed within various fat depots, including interscapular BAT (iBAT), inguinal WAT (iWAT), epididymal WAT (eWAT), and bone marrow (BM) in adult mice (Figure 1A). Since adipose tissues possess multiple types of non-adipocytes (Cinti, 2005), and the nuclei are often squeezed at the edge of mature adipocytes, it is difficult to determine the exact hosts of the GFP$^+$ nuclei in adipose tissues. To confirm that these Wnt/β-catenin positive cells are indeed adipocytes, we created a *Tcf/Lef-CreERT2* transgenic allele in which the *CreERT2* cassette was placed under the control of the same regulatory elements as that used in the *T/L-GFP* allele (Figure S1A). This *Tcf/Lef-CreERT2* allele, upon compounding with *Rosa26R*^{mTmG} reporter allele followed by tamoxifen administration, indelibly labeled the membrane of a fraction of adipocytes, as seen in freshly isolated cells and in sectioned iWAT and iBAT (Figures S1B, S1C, S1E, and S1F). Moreover, addition of the *T/L-GFP* allele to *Tcf/Lef-CreERT2*;*Rosa26R*^{mTmG} mice produced adipocytes that were tagged by both membrane-bound and nucleus-localized GFP (Figure S1D). Therefore, we identified a population of adipocytes that displays active Wnt/β-catenin cascade, and accordingly, we referred to these cells as Wnt$^+$ adipocytes.

To chart a census of Wnt$^+$ adipocytes within distinct mouse fat depots, we quantified Wnt$^+$ fat cells in *T/L-GFP* mice. We observed that the adipocytes expressing nuclear GFP count for various percentages of total fat cells in different fat depots, with the highest level (17.02% ± 3.06%) in iBAT, the lowest one (1.28% ± 0.56%) in eWAT, and relatively abundant percentage (6.86% ± 0.98%) in iWAT, a representative beiging site (Nedergaard and Cannon, 2014), of adult male mice (Figure 1C). In addition, Wnt$^+$ adipocytes could be detected as early as embryonic day 17.5 (E17.5) (Figures S1G and S1H) and the proportions varied in different fat depots over the course of postnatal stages (Figures S1K and S1L). Interestingly, sex and age appeared to have impact on the amounts of Wnt$^+$ adipocytes, as

the percentage of Wnt$^+$ adipocyte in female fat depots was around half as compared to their male counterparts and was dramatically reduced in aged male mice (Figures S1I-S1L).

Characterization of Wnt$^+$ Adipocytes Demonstrates Their Distinct Lineage Origin and Cellular Intrinsic Wnt/β-catenin Signaling Activity

To characterize Wnt$^+$ adipocytes, we set out to determine if the resident SVF cells within adipose tissues constitute the source of Wnt$^+$ adipocytes. Using standard white fat pro-adipogenic induction protocol, we readily induced Wnt$^+$ adipocytes *in vitro* from SVFs derived from iBAT, iWAT, eWAT, as well as BM stroma, as confirmed by staining of the general adipocyte marker Adiponectin, and also surprisingly by the co-expression of Pparγ that is believed to be suppressed by the canonical Wnt signaling (Figures 1B and 1E). The induced Wnt$^+$ adipocytes exhibited similar morphology compared to Wnt$^-$ (non-GFP labeled) ones and also made up a very similar percentage of total induced fat cells as they are present in their corresponding fat depot (Figure 1D), suggesting that the Wnt$^+$ adipocytes we observed *in vivo* are derived from the adipogenic precursors among SVFs. Given the fact that Wnt$^+$ adipocytes are present in embryos, we asked if embryonic mesenchymal stem cells can differentiate to Wnt$^+$ adipocytes as well. Notably, we could induce E13.5 mouse embryonic fibroblasts (MEFs) to differentiate into Wnt$^+$ adipocytes *in vitro* (Figure S1M), indicating an early developmental origin of Wnt$^+$ adipocytes.

To determine if Wnt$^+$ adipocytes would also exist in humans, we transfected human primary bone marrow stromal cells (BMSCs) with an mCherry-expressing lentiviral vector carrying a *TCF/Lef:H2B-GFP* reporter cassette (Figure S2A) and then cultured these cells with pro-differentiation medium. As the positive control, pre-osteocytes/osteocytes

differentiated from infected BMSCs under pro-osteogenic conditions exhibited overlapped mCherry expression and nuclear Wnt/β-catenin signaling activity (Figure S2B), validating the effectiveness of the transduction system. Importantly, under the pro-adipogenic medium, we observed GFP-tagged adipocytes from the infected BMSCs (Figure 1F), indicating the differentiation of Wnt^+ adipocytes from human stromal cells. Together, these results suggest that Wnt^+ fat cells appear to constitute a widespread adipocyte population that originates from embryonic stage and exists in mice and possibly in humans.

To address how Wnt^+ adipocytes develop during adipogenesis, we conducted real-time monitoring on behaviors of induced Wnt^+ adipocytes *in vitro*. No Wnt/β-catenin signaling activity was seen in SVFs in culture prior to pro-adipogenic induction (Figure 2A). Nuclear GFP expression was initially detected in differentiated adipocytes (defined by the presence of lipid droplets) after 2-day adipogenic induction and the GFP signal was sustained once it was activated (Figure 2A), indicating that Wnt/β-catenin signaling does not transiently appear but persists in Wnt^+ adipocytes. Interestingly, after 7-day differentiation, we observed colonized Wnt^+ and Wnt^- adipocytes, respectively, induced from primary BMSCs of *T/L-GFP* mice, suggesting distinct cell lineages of these two different adipocyte populations (Figure S3A). This conclusion is supported by the observation that induced Wnt^+ and Wnt^- adipocytes, after separation by fluorescence-activated cell sorting (FACS) and subsequent 4-day in culture, did not convert mutually (Figure 2B). The consistent Wnt/β-catenin signaling within Wnt^+ adipocyte thus represents an intrinsic cascade activity.

To ensure that the GFP expression in *T/L-GFP* adipocytes both *in vivo* and *in vitro* represents authentic Wnt/β-catenin signaling activity, we first confirmed the presence of active β-catenin and Tcf/Lef1 in the nuclei of Wnt^+ adipocytes within adipose tissues (Figures S3B and S3C). We further found that Tcf7l2 expression was largely overlapped

(~91%) with Wnt$^+$ adipocytes, whereas other Tcf proteins (Tcf1, Tcf3, and Lef1) were barely seen in Wnt$^+$ adipocytes (data not shown). We next conducted knockdown experiments using short interfering RNA (siRNA) targeting *Ctnnb1* followed by real-time monitoring. As shown in Figure 2C, *Ctnnb1* knockdown in differentiated Wnt$^+$ adipocytes virtually quenched the GFP signals, followed by cell shrinkage. Moreover, while DKK1 and IWP-2, both canonical Wnt receptor antagonists, failed to, LF3, a molecule that disrupts the interaction between β-catenin and Tcf7l2 (Fang et al., 2016), did inhibit Wnt/β-catenin signaling activity in precursors under pro-adipogenic conditions (Figures 2D and S3D-S3F). This observation indicates that the activation of the cellular intrinsic Wnt/β-catenin signaling in Wnt$^+$ adipocytes is ligand- and receptor-independent. Remarkably, pharmacological inhibition of Wnt/β-catenin signaling by LF3 also resulted in an overall impaired/delayed adipogenic maturation of SVF-derived adipocytes in a dose-dependent manner (Figure 2D), suggesting a potentially functional importance of the intracellular Wnt/β-catenin signaling in adipogenesis.

To further define the specific roles of Wnt/β-catenin signaling in Wnt$^+$ and Wnt$^-$ adipocytes, we immortalized SVF cells (mBaSVF) derived from iBAT of *T/L-GFP* mouse. By serial limited dilutions, we isolated two Wnt$^+$ (GFPpos-1 and GFPpos-2) and two Wnt$^-$ (GFPneg-1 and GFPneg-2) adipocyte precursor cell lines from mBaSVF cells, respectively. Of note, LF3 treatment of induced Wnt$^+$ adipocytes from both GFPpos-1 and GFPpos-2 cell lines quenched GFP expression in the first day of culture (Figure 2E), followed by massive cell death in the second day (Figure 2F). By contrast, LF3 administration to induced Wnt$^-$ adipocytes from precursor cell lines did not affect cell viability but slowed down the maturation of Wnt$^-$ adipocytes (Figures S3G-S3J) similar to that seen in SVF induced adipocytes (Figure 2D). However, such LF3-treated Wnt$^-$ adipocytes, once returned to normal pro-adipogenic medium, resumed full adipogenic capacity compared to controls

(Figures 2G and 2H), indicating that LF3 treatment does not impair but delays the maturation of Wnt$^-$ adipocytes. As controls, the same dose of LF3 showed no impacts on uninduced Wnt$^+$ and Wnt$^-$ precursor cell lines (Figure S5E).

Wnt$^+$ Adipocytes are Diverse from Conventional Ones with Distinct Molecular and Genomic Characteristics

To further distinguish Wnt$^+$ adipocytes from Wnt$^-$ fat cells and explore the global diversity at molecular and genomic levels, we performed single-cell RNA sequencing analysis (scRNA-seq) and single-cell assay for transposase-accessible chromatin sequencing (scATAC-seq) on FACS separated Wnt$^+$ and Wnt$^-$ adipocytes induced from iWAT- and iBAT-derived SVF cells, respectively (Figure 3A). After filtering for quality and excluding nonadipocytes (negative for *Adiponectin* expression), bioinformatic analyses classified the input Wnt$^+$ and Wnt$^-$ adipocytes into distinct clusters, indicating two different types of adipocytes (Figures 3B-3E and S4A-S4F). Notably, although the mRNA expression of *Ucp1* was undetectable based on our single-cell transcriptomic data, violin plots showed that several thermogenesis-related genes such as *Cox8b* and *Elovl3* were present at significantly higher levels in Wnt$^+$ adipocytes that were subject to the white fat differentiation condition without browning stimuli (Figure 3F), indicative of potentially thermogenic character. Moreover, *Cyp2e1*, a molecule identified as a marker gene in thermogenic regulation (Sun et al., 2020b), and *Cidea* were exclusively expressed in a subset of Wnt$^+$ adipocytes induced from iWAT- and iBAT-derived SVFs, as confirmed by immunofluorescent staining (Figures 3D-3F, S4G, and S4H). These facts link Wnt$^+$ adipocytes to thermogenic function in adipose tissues. Enrichment pathway analyses of differentially expressed genes (DEGs) also suggests the primary functions of this population of adipocytes in the regulation of adipogenesis, fatty acid metabolism, and mTORC1 signaling (Figures 3G-3J). Thus, these results demonstrated

that this novel population of Wnt/β-catenin signaling driven adipocytes is distinct from the classical adipocytes at molecular and genomic levels.

Insulin/AKT/mTORC1 Signaling Is Required for Activation of Intracellular Wnt/β-catenin Cascade within Wnt$^+$ Adipocytes

PI3K/AKT/mTOR signaling modulated by insulin is manifested for promoting cytoplasmic β-catenin accumulation through GSK-3β phosphorylation (Hermida et al., 2017; Schakman et al., 2008). This notion upon signaling crosstalk drew our attention because insulin signaling plays pivotal roles in mediating adipogenic differentiation and functionality and our enrichment pathway analyses also implicate a link to mTORC1 signaling (Figures 3G-3J). Accordingly, we first assessed AKT signaling activities in induced Wnt$^+$ and Wnt$^-$ adipocytes. Immunoblot assay showed that GFPpos-derived Wnt$^+$ adipocytes exhibited markedly higher levels of AKT phosphorylation than that from GFPneg-derived Wnt$^-$ adipocytes and from mBaSVF-induced adipocytes as unbiased fat cell control (Figure 4A). Phosphorylated GSK-3β and 4E-BP1 (Eukaryotic translation initiation factor 4E-binding protein 1), a known substrate of mTOR signaling pathway (Beretta et al., 1996), were also found preferentially higher in Wnt$^+$ adipocytes as compared to controls (Figure 4B). These results demonstrate enhanced AKT/mTORC1 cascade activity and insulin sensitivity in Wnt$^+$ fat cells.

To test if AKT/mTOR signaling is responsible for intracellular Wnt/β-catenin signaling activation in Wnt$^+$ adipocytes, we started with treating iBAT-derived SVF cells with LY294002, a selective PI3K signaling antagonist, under pro-adipogenic conditions. Again, dramatically reduced number of Wnt$^+$ adipocytes and blunted adipogenesis were observed in a dose-dependent manner (Figures S5A and S5B). Consistently, LY294002 administration to

GFPpos-induced Wnt$^+$ adipocytes eliminated GFP expression and caused substantial cell death subsequently but did not impact on the survival of GFPneg-derived adipocytes (Figures 4C, 4D, and S5C-S5E). To determine a causal role of mTOR signaling in the intracellular activation of Wnt/β-catenin signaling in adipocytes *in vivo*, we subjected *T/L-GFP* adult mice to an mTOR-specific antagonist Temsirolimus treatment, which dramatically reduced Wnt$^+$ adipocyte number in both iWAT and iBAT compared to vehicle-injected controls (Figures 4E and 4F). These results demonstrate the dependence of the Wnt/β-catenin signaling activity in adipocytes on AKT/mTOR signaling, which is required for cell survival.

To further validate the requirement of insulin signaling in Wnt$^+$ adipocyte development *in vivo*, we employed *Ins2^{Akita}* mice (the so-called Akita mice) in which insulin secretion is profoundly impaired due to genetic defect in the insulin 2 gene (Yoshioka et al., 1997) by crossing them to *T/L-GFP* mice. As expected, Wnt$^+$ adipocytes were completely absent in iWAT and substantially reduced in number in iBAT (3.34% ± 0.55%) of 8-week-old male Akita mice (Figures 4G and 4H), demonstrating an indispensable effect of insulin-induced AKT/mTOR signaling on Wnt$^+$ adipocytes differentiation.

Wnt$^+$ Adipocytes Are Required for Initiating Adaptive Thermogenesis in Both Cell Autonomous and Non-cell Autonomous Manners

The potentially highly metabolic and thermogenic characters in Wnt$^+$ adipocytes prompted us to investigate the adaptive thermogenic role of Wnt$^+$ adipocytes. We started with the examination of mitochondrial activities in SVF-derived adipocytes *in vitro* and found that Wnt$^+$ adipocytes, along with those closely adjacent Wnt$^-$ ones, exhibited pronounced lower levels of mitochondrial membrane potential, indicative of higher uncoupling rate, as compared to those Wnt$^-$ fat cells located relatively away from Wnt$^+$ adipocytes (Figures 5A

and 5B). In addition, significantly higher levels of oxygen consumption rate (OCR) were detected in GFPpos-induced Wnt$^+$ adipocytes as compared to those GFPneg-derived Wnt$^-$ adipocytes and mBaSVF-induced fat cells (Figures 5C, S6A, and S6B), further demonstrating a higher mitochondrial respiration capacity of Wnt$^+$ adipocytes.

To explore the possible involvement of Wnt$^+$ adipocytes in adaptive thermogenesis *in vivo*, adult *T/L-GFP* male mice were subjected to 6ºC temperature for 2 days to initiate beiging. After cold exposure, we observed the presence of a subset of UCP1-expressing beige adipocytes that were also GFP-positive (Figure S6C), demonstrating that a portion of beige fat cells arises from Wnt$^+$ adipocyte lineage. Similar results were seen in mice treated with β3-adrenergic receptor agonist CL316,243 (Figure S6C). However, despite that the proportion of Wnt$^+$ adipocytes in iWAT appeared unaltered in response to cold stress or β3-adrenergic receptor agonist treatments (Figure S6D). Remarkably, as cold exposure was prolonged to 4 days, the number of Wnt$^-$ beige adipocytes increased dramatically, but the majority of, if not all, UCP1-labeled Wnt$^-$ beige adipocytes were found present neighboring to Wnt$^+$ adipocytes (Figure 5D). UCP1$^+$/Wnt$^-$ beige adipocytes were rarely seen away from Wnt$^+$ adipocytes within iWAT, implicating a regulatory role of Wnt$^+$ adipocytes in beige fat biogenesis. Together with the results from mitochondrial activity assays, these observations suggest a paracrine function of Wnt$^+$ adipocytes in modulating beige fat formation.

To determine whether those Wnt$^+$ beige adipocytes are converted directly from Wnt$^+$ adipocytes under cold conditions, we conducted lineage-tracing studies using *Tcf/Lef-CreERT2*;*Rosa26R*^{mTmG} mice. After pre-treatment with tamoxifen and a 2-week washout at ambient temperature, *Tcf/Lef-CreERT2*;*Rosa26R*^{mTmG} mice were subjected to cold challenge for 4 days. These mice manifested the presence of mGFP and UCP1 co-labeled adipocytes in iWAT (Figure 5E), providing unambiguous evidence for the cell autonomous contribution of Wnt$^+$ adipocytes to beiging.

To establish a non-cell autonomous role for Wnt$^+$ adipocytes in beige fat biogenesis, we generated a *Fabp4-Flex-DTA* mouse model (Figure S6E), a diphtheria-toxin-induced depletion system that allows targeted ablation of Wnt$^+$ adipocytes upon crossing to *Tcf/Lef-CreERT2* mice (*T/L-DTA* mice) and tamoxifen administration (Figure S6F). Wnt$^+$ adipocyte-ablated mice and littermate controls (*Fabp4-Flex-DTA* mice) were then challenged by 6ºC temperature. We first measured the core body temperature of each mouse and found that about 31% *T/L-DTA* mice (5 of 16 mice) developed hypothermia (below 34.5ºC) within 60 hours, with the rest of the *T/L-DTA* mice exhibiting comparable core body temperature as the controls (Table S4). We next examined if the formation of cold-induced beige fat in iWAT of *T/L-DTA* mice would be blunted. After 4-day cold stress, DTA-induced ablation of Wnt$^+$ adipocytes led to substantially reduced UCP1-expressing beige adipocytes compared to control littermates (Figure 5F). This markedly attenuated UCP1 expression persisted even after 2 weeks of cold adaptation (Figure S6G). The compromised beiging process in iWAT was verified by remarkably decreased expression levels of thermogenic genes assessed by qRT-PCR and western blotting (Figures 5G and 5H). Since the mRNA levels of the pan-adipogenic marker *Adipoq* (*Adiponectin*) appeared similarly between the genotypes (Figure S6H), it was used as internal reference. As shown in Figure 5G, loss of Wnt$^+$ adipocytes in *T/L-DTA* mice caused significantly suppressed expression of thermogenesis-related genes specifically but not those general adipogenic markers in iWAT. Because Akita mice lack Wnt$^+$ adipocytes in iWAT (Figures 4G and 4H), similar to *T/L-DTA* ones, we tested whether Akita mice also display an impaired adaptive thermogenic capacity by challenging Akita mice at 6ºC. Immunofluorescence staining further validated that cold-induced UCP1$^+$ cells were largely absent in iWAT of Akita mice (Figure 5I). Collectively, these results demonstrate an essential role of Wnt$^+$ adipocytes in initiating beige adipogenesis under cold conditions via non-cell autonomous effect.

Wnt$^+$ Adipocytes Enhance Systemic Glucose Handling in Mice

Given that the presence of Wnt$^+$ adipocyte is highly dependent on insulin signaling, we set to evaluate the potential physiological impact of Wnt$^+$ adipocytes on whole-body glucose homeostasis. We started with loss-of-function studies by using *T/L-DTA* mice, which, under regular chow diet, were subjected to glucose tolerance assays 24 hrs after tamoxifen administration. The results showed clearly that *T/L-DTA* mice displayed impaired glucose handling competence as compared to controls despite similar basal glucose levels (Figure 6A), indicating a requirement for Wnt$^+$ adipocytes in handing systemic glucose. We next took gain-of-function approach to test if Wnt$^+$ adipocytes are sufficient to enhance systemic glucose utilization. For this purpose, immortalized GFPpos and mBaSVF cells were induced to become adipogenic commitment after 2-day in pro-adipogenic medium. Committed cells were mixed with Matrigel and implanted into the left abdomen subcutaneous layer of wild-type C57BL/6J mice under regular chow (Figure 6B). These implanted cells differentiated into fully mature adipocytes readily and formed vascularized adipose tissues *in vivo* within 2-week (Figures 6C and 6D). Glucose tolerance assays were performed on mice 2-week after cell implantation. The results showed that mice bearing implanted Wnt$^+$ adipocytes exhibited a significantly enhanced glucose tolerance as compared to mice receiving mBaSVF-derived adipocytes (Figure 6E). Taken together, these results provide appealing evidence for the beneficial impact of Wnt$^+$ adipocytes in systemic glucose homeostasis.

Discussion

Over the past few decades, numerous studies support the notion that the canonical Wnt signaling pathway functions as a powerful suppressor of adipogenesis (Longo et al., 2004;

Ross et al., 2000; Waki et al., 2007). Our current studies challenge the conventional dogma conceptually by presenting direct evidence for the existence of a population of Wnt/β-catenin signaling driven adipocytes, namely Wnt^+ adipocytes, revealing the diversity of adipocytes. We further demonstrated that the Wnt/β-catenin signaling is activated intracellularly via signaling crosstalk, in this case, AKT/mTOR signaling. Although if AKT/mTOR signaling cascade can activate canonical Wnt signaling remains contradictory (Baryawno et al., 2010; Cabrae et al., 2020; Ng et al., 2009; Palsgaard et al., 2012; Prossomariti et al., 2020; Zhang et al., 2013), it appears to be cell-type dependent. This population of Wnt^+ adipocytes was neglected, presumably because most of the previous studies were performed in aggregates of mixed cell types through Wnt ligand- and receptor-dependent manners. Importantly, we showed that the intracellular Wnt/β-catenin signaling indeed has an overall impact on adipogenesis, as supported by its requirement for the survival of Wnt^+ adipocytes and maturation of Wnt^- adipocytes, though the underlying mechanisms warrant further investigation. Since AKT/mTOR signaling is known to promote lipid storage (Laplante and Sabatini, 2009) and is required for the activation of the intracellular Wnt/β-catenin signaling (this study), it is possible that Wnt^- adipocytes also possess basal activity of Wnt/β-catenin signaling that is critical for lipid accumulation. This hypothesis is consistent with a prior study that silencing *Tcf7l2* leads to blockade of adipogenesis (Chen et al., 2018).

Our single-cell sequencing data showed that Wnt^+ adipocytes, as compared to Wnt^- adipocytes induced from SVF cells of iWAT and iBAT origins, exhibit distinct signatures at molecular and genomic levels, further supporting the Wnt^+ adipocytes as a unique subpopulation of fat cells in mammals. However, since FACS-based selection of mature adipocytes presents a huge challenge, we had to perform sequencing on *in vitro* cultured cells that were not under their true physiological status. We have attempted to conduct single nucleus RNA sequencing (snRNA-seq) on mature adipocytes isolated from adipose tissues.

However, unlike the previous successful studies in which adipocyte nuclei were isolated from adipose tissues simply by one-step enzyme digestion prior to snRNA-seq (Rajbhandari et al., 2019; Sarvari et al., 2020; Sun et al., 2020b), we were not able to obtain desired results due to nuclear membrane breakage after enzyme digestion and following FACS separation of Wnt^+ and Wnt^- adipocyte nuclei. Nevertheless, under the standard white fat pro-adipogenic induction, SVF-induced Wnt^+ adipocytes, but not Wnt^- adipocytes, express several brown/beige fat-selective genes, mirroring the thermogenic feature. In addition, pathway analyses indicate highly enriched insulin signaling pathway in Wnt^+ adipocytes, as compared to Wnt^- fat cells, consistent with the intracellular activation of Wnt/β-catenin signaling by AKT/mTOR signaling cascade. While many subpopulations of heterogeneous pre-adipocytes/adipocytes have been identified, the classification of each subset replies mainly on the expression of specific genes such as cell surface markers (Hepler et al., 2018; Oguri et al., 2020; Schwalie et al., 2018; Wu et al., 2012). Our current studies, based on the stable feature of an intrinsic cellular signaling identity, provide a new revenue for taxonomy of adipocytes.

In line with their thermogenic feature, as revealed by gene expression profiling, our studies have further uncovered a key role of Wnt^+ adipocytes in adaptive thermogenesis of adipose tissues. First, Wnt^+ adipocytes represent at least one of the cell populations that can convert into beige adipocytes directly following cold stress. Interestingly, a conversion of mature white adipocyte to reprogrammed beige characteristics has been postulated to occur predominantly in the “dormant” or “latent” beige fat (i.e., thermogenic inactive state of UCP1 lineage adipocytes within WAT depots), which was thought to form initially through *de novo* beige adipogenesis from progenitors during postnatal development (Paulo and Wang, 2019; Shao et al., 2019). Because UCP1 expression within iWAT starts at postnatal day 14 independent of environmental temperature (Wu et al., 2020), dormant beige adipocytes appear much later in development than Wnt^+ adipocytes that can be found in embryonic

stage. Therefore, together with the observations that Wnt$^+$ and Wnt$^-$ adipocytes do not convert mutually in cell culture, our findings suggest that Wnt$^+$ adipocytes differ from dormant beige cells and represent a population of adipocytes that retain the cellular plasticity and are capable of converting to beige adipocytes directly. Second, it is worth noting that Wnt$^+$ adipocytes are also required for beige adipogenesis. Upon cold exposure, UCP1$^+$/Wnt$^-$ beige fat emerges largely surrounding Wnt$^+$ adipocytes, implicating that Wnt$^+$ adipocytes serve as a beiging initiator in a paracrine manner. Remarkably, using a targeted cell ablation system, we showed that depletion of Wnt$^+$ fat cells in mice leads to failed beige biogenesis in iWAT in response to cold stress. Severely impaired beiging phenotype was also seen in iWAT of Akita mice that lack Wnt$^+$ adipocytes. These observations underscore the functional importance of Wnt$^+$ adipocytes in triggering adaptive thermogenic program of adipose tissue. Despite that the critical factors produced by Wnt$^+$ adipocytes to trigger beige adipogenesis remain completely unknown, we conclude that Wnt$^+$ adipocytes act as a key initiator in beige biogenesis through both cell autonomous (direct conversion) and non-cell autonomous (recruitment) manners.

The significant contributions of beige adipocytes to improving whole-body glucose homeostasis and countering diet-induced obesity have been well documented (Bartelt and Heeren, 2014; Crane *et al.*, 2015; Harms and Seale, 2013). GWAS has also linked genetic variations in *TCF7L2*, a key component of canonical Wnt pathway, to type 2 diabetes in humans (Chen et al., 2018; Voight et al., 2010). We thus speculated that Wnt$^+$ adipocytes, driven by insulin/AKT signaling and functioning as beiging initiator in mice, represent a population of beneficial adipocytes and hold the therapeutic potential for metabolic diseases. Accordingly, our results demonstrate whole-body glucose intolerance in mice with targeted ablation of Wnt$^+$ adipocytes but notably enhanced glucose utilization in mice receiving implantation of exogenously induced Wnt$^+$ adipocytes, highlighting Wnt$^+$ adipocytes as a

therapeutically appealing candidate of cell source to restore systemic glucose homeostasis. The evidence that Wnt^+ adipocytes could be induced from human primary BMSCs opens a door for future translational research. For such purpose, a few urgent questions need to be addressed: 1) if Wnt^+ adipocytes serve as the primary target of insulin to modulate glucose homeostasis; 2) what are critical factors/adipokines produced by Wnt^+ adipocytes; 3) and how these factors/adipokines are presented and exert their functions.

ACKNOWLEDGEMENTS

We thank members of the Chen Lab for providing technical advice and sharing reagents. This work was supported by a Carol Lavin Bernick Faculty Grant from Tulane University, the John L. and Mary Wright Ebaugh Endowed Chair Fund, and a grant (R01DK128907) from the NIH to Y.C. T.Y. was supported by an American Heart Association Predoctoral Fellowship (20PRE35040002).

AUTHOR CONTRIBUTIONS

Z.L., T.C., W.T. and Y.C. conceived the study and designed experiments. D.B. helped to design the initial experiments and provide mentoring and intellectual advice during the study. Z.L., T.C., S.Z., T.Y. performed experiments. Y.G. and H.D. helped to analyze bioinformatic data. Z.L., T.C., S.Z., W.T. and Y.C. collected, analyzed, and interpreted data. Z.L. and T.C. wrote manuscript, and Z.L., T.C., W.T. and Y.C edited the manuscript.

DECLARATION OF INTERESTS

The authors declare no competing interests.

FIGURE LEGENDS

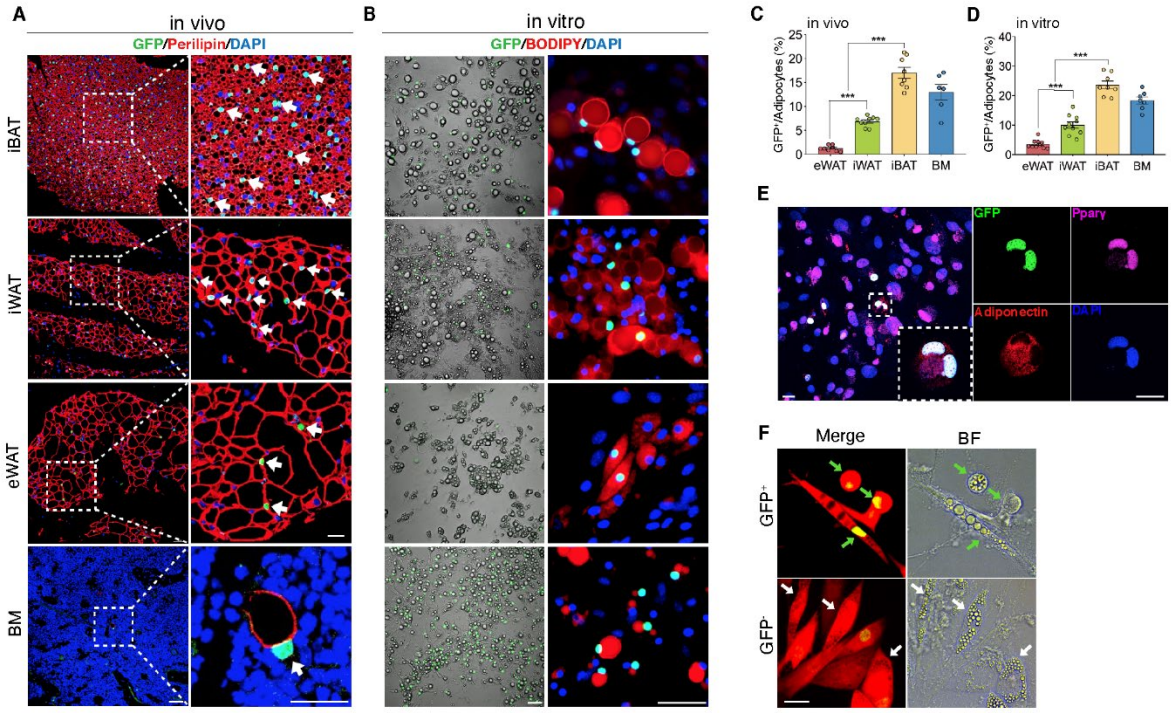

Figure 1. The existence of adipocytes exhibiting active Wnt/β-catenin signaling

(A and B) Immunofluorescent and microscopy images of active Wnt/β-catenin signaling *in vivo* (A) and *in vitro* (B), indicated by GFP expression from the *TCF/Lef:H2B-GFP* allele, in adipocytes marked by Perilipin or BODIPY (red). Nuclei were stained with DAPI (blue). Scale bars, 50 μm; close-up scale bars, 20 μm.

(C) Quantification of Wnt^+ adipocytes among total adipocytes in various fat depots of adult male mice in (A). The levels of mRNA expression are normalized to that of *36B4*. n = 6-9 mice.

(D) Quantification of Wnt^+ adipocytes among total adipocytes induced from SVF cells derived from adult male fat depots and BM stroma in (B). mRNA expression relative to *36B4*. n = 7-10 independent experiments.

(E) Immunofluorescent staining of Pparγ (purple) and Adiponectin (red) in cultured GFP^+ adipocytes derived from bone marrow in (B). n = 3 independent experiments. Scale bars, 20 μm.

(F) Representative images of GFP^+ (green arrows) and GFP^- (white arrows) adipocytes induced from human bone marrow stromal cells infected with *TCF/Lef:H2B-GFP* reporter lentiviral virus. n = 2 independent experiments, 3 independent wells each. Scale bar, 20 μm.

Data are mean ± s.e.m., ***$P < 0.001$, one-way ANOVA followed by Tukey's test. See also Figures S1 and S2.

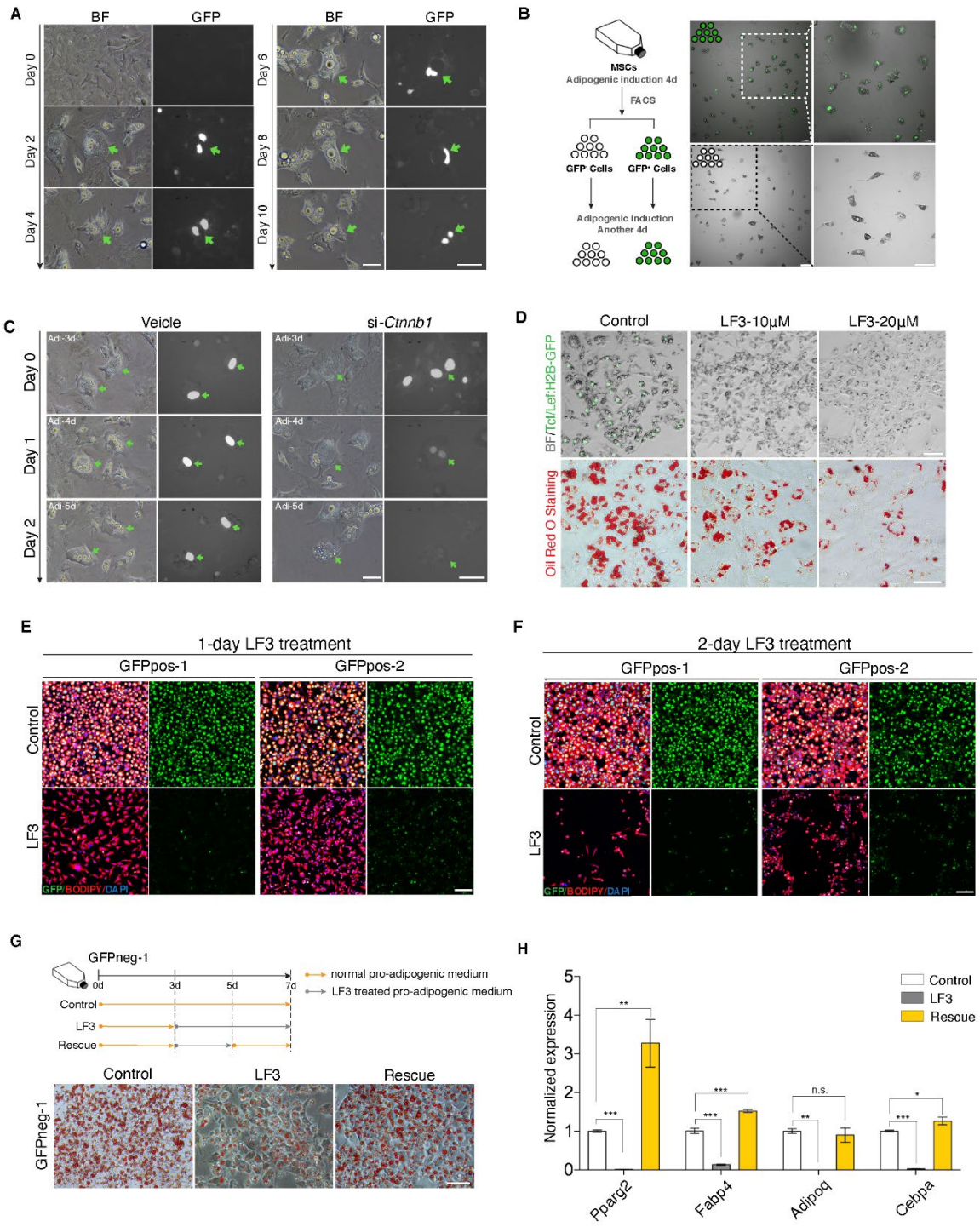

Figure 2. Characterization of mouse Wnt$^+$ adipocytes

(A) Real-time monitoring microscopy images of Wnt$^+$ adipocytes during adipogenesis, which were induced from BMSCs of *T/L-GFP* mice. n = 3 independent experiments. Scale bar, 50 μm.

(B) Schematic of the experiments and microscopy images of separated Wnt$^+$ and Wnt$^-$ adipocytes by FACS. n = 3 independent experiments. Scale bars, 100 μm.

(C) Time-lapse microscopy images of induced Wnt^+ adipocytes from BMSCs of *T/L-GFP* mice with *Ctnnb1* and control siRNA-mediated knockdown. $n = 2$ independent experiments, 3 independent wells each. Scale bars, 50 μm.

(D) Microscopy images and Oil Red O staining of Wnt^+ adipocytes induced from iBAT-derived SVF cells of *T/L-GFP* mice with control and LF3 treatment in different doses. $n = 5$ independent experiments. Scale bars, 50 μm.

(E and F) Immunofluorescent images of Wnt^+ adipocytes induced from two independent cell lines (GFPpos-1 and -2) with LF3 treatment (50 μM) for one (E) and two days (F), respectively. LF3 was added into the medium after 3-day pro-adipogenic induction. Note that by 1-day LF3 administration, GFP signals were significantly quenched in Wnt^+ adipocytes, along with obviously reduced cell number. By 2-day LF3 administration, remarkable cell death of Wnt^+ adipocytes was seen, compared to controls. Scale bar, 100 μm.

(G) Schematic of rescue experiment and microscopy images of Oil Red O staining in adipocytes induced from GFPneg-1 cell line with LF3 treatment. $n = 3$ independent experiments. Scale bar, 50 μm.

(H) Quantitative RT-PCR analysis of the expression of adipogenic genes in (G). The levels of mRNA expression are normalized to that of *36B4*.

Data are mean ± s.e.m., $*P < 0.05$, $**P < 0.01$; $***P < 0.001$, n.s., not significant, one-way ANOVA followed by Tukey's test. See also Figure S3.

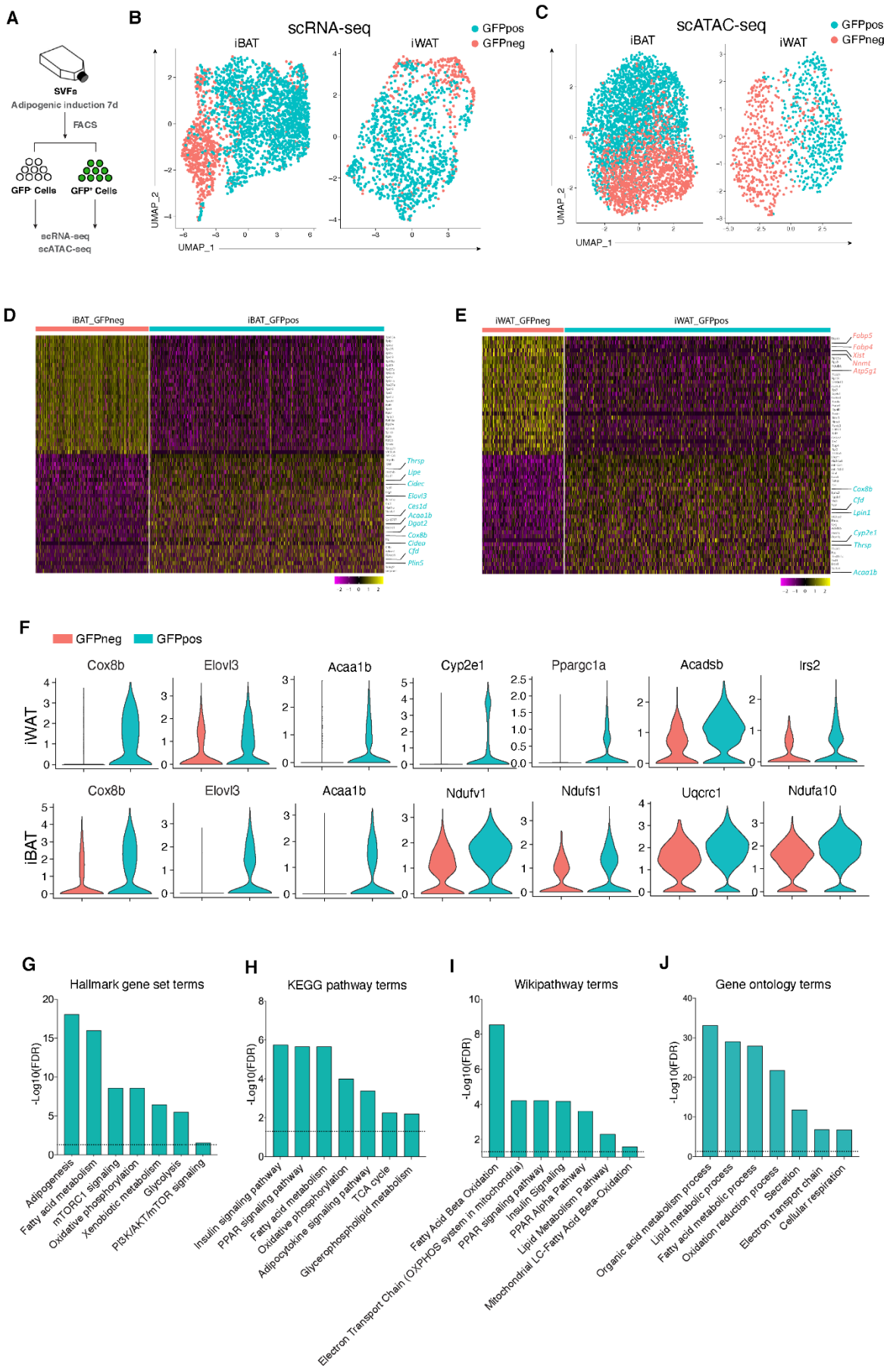
A
SVFs
Adipogenic induction 7d
FACS
GFP- Cells
GFP+ Cells
scRNA-seq
scATAC-seq
B
scRNA-seq
iBAT
iWAT
GFPpos
GFPneg
UMAP_1
UMAP_2
C
scATAC-seq
iBAT
iWAT
GFPpos
GFPneg
UMAP_1
UMAP_2
D
iBAT_GFPneg
iBAT_GFPpos
Thrsp
Ucp1
Cidec
Elovl3
Cas1d
Acaa1b
Dgat2
Cox8b
Cidea
Cfd
Plin5
E
iWAT_GFPneg
iWAT_GFPpos
Fabp5
Fabp4
Kist
Nnmt
Atp5g1
Cox8b
Cfd
Lpin1
Cyp2e1
Thrsp
Acaa1b
F
GFPneg
GFPpos
iWAT
Cox8b
Elovl3
Acaa1b
Cyp2e1
Ppargc1a
Acadsb
Irs2
iBAT
Cox8b
Elovl3
Acaa1b
Ndufv1
Ndufs1
Uqcrc1
Ndufa10
G
Hallmark gene set terms
-Log10(FDR)
Adipogenesis
Fatty acid metabolism
mTORC1 signaling
Oxidative phosphorylation
Xenobiotic metabolism
Glycolysis
PI3K/AKT/mTOR signaling
H
KEGG pathway terms
-Log10(FDR)
Insulin signaling pathway
PPAR signaling pathway
Fatty acid metabolism
Oxidative phosphorylation
Adipocytokine signaling pathway
Glycerophospholipid metabolism
TCA cycle
I
Wikipathway terms
-Log10(FDR)
Fatty Acid Beta Oxidation
Electron Transport Chain (OXPHOS system in mitochondria)
PPAR signaling pathway
Insulin Signaling
PPAR Alpha Pathway
Lipid Metabolism Pathway
Mitochondrial LC-Fatty Acid Beta-Oxidation
J
Gene ontology terms
-Log10(FDR)
Organic acid metabolism process
Lipid metabolic process
Fatty acid metabolic process
Oxidation reduction process
Secretion
Electron transport chain
Cellular respiration

1

Figure 3. Distinct molecular and genomic signatures of Wnt$^+$ and Wnt$^-$ adipocytes

(A) Schematic of scRNA-seq and scATAC-seq experiments on SVF-induced adipocytes.

(B) Uniform Manifold Approximation and Projection (UMAP) visualization of 2,537 adipocytes from iBAT (1,710 GFP$^+$ and 827 GFP$^-$) and 1,345 adipocytes from iWAT (984 GFP$^+$ and 361 GFP$^-$) in scRNA-seq.

(C) UMAP visualization of 4,302 adipocytes from iBAT (1,727 GFP$^+$ and 2,575 GFP$^-$) and 1,383 adipocytes from iWAT (562 GFP$^+$ and 821 GFP$^-$) in scATAC-seq.

(D and E) Heat maps of expression of top 30 signature genes (Table S2) in iBAT- (B) and iWAT-derived (C) Wnt$^+$ and Wnt$^-$ adipocytes in scRNA-seq.

(F) Violin plots of induced Wnt$^+$ and Wnt$^-$ adipocytes showing the distribution of normalized expression values of some representative genes in scRNA-seq.

(G-J) Hallmark gene sets (G), KEGG pathway (H), Wikipathway (I), and GO Biological Processes ontology (J) analyses of DEGs enriched in iWAT-derived Wnt$^+$ adipocytes in scRNA-seq (Table S3).

Also see Figure S4.

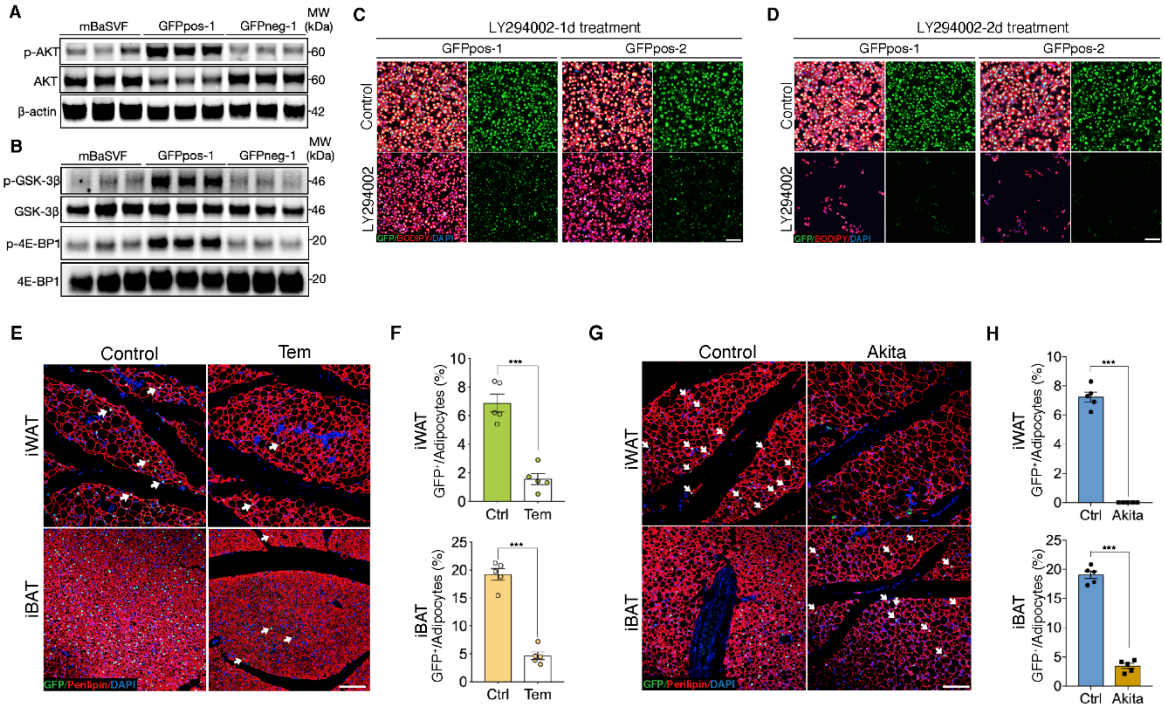

Figure 4. AKT/mTOR cascade is indispensable to trigger intracellular Wnt/β-catenin signaling in Wnt$^+$ adipocytes

(A) Western blot analysis showing protein levels of AKT, phosphorylated AKT, and β-actin in adipocytes induced from mBaSVF, GFPpos-1, and GFPneg-1 cell lines. n = 3 independent experiments.

(B) Western blot analysis showing protein levels of GSK-3β, phosphorylated GSK-3β, 4E-BP1, and phosphorylated 4E-BP1 in adipocytes induced from mBaSVF, GFPpos-1, and GFPneg-1 cell lines. n = 3 independent experiments.

(C and D) Immunofluorescent images of Wnt$^+$ and Wnt$^-$ adipocytes induced from two independent precursor cell lines (GFPpos-1 and -2) with LY294002 treatment (14 μM) for one (C) and two days (D), respectively. LY294002 was added into the medium after 3-day pro-adipogenic induction. LY294002 treatment diminished GFP signals prior to causing marked cell death in Wnt$^+$ adipocytes. n = 5 independent experiments. Scale bar, 100 μm.

(E) Immunofluorescent images of iWAT and iBAT of *T/L-GFP* mice treated with or without Temsirolimus (Tem). n = 5 mice. Scale bar, 100 μm.

(F) Quantification of Wnt$^+$ adipocytes among total adipocytes in (E).

(G) Immunofluorescent images of iWAT and iBAT of male *Ins2^{Akita}*;*T/L-GFP* mice at 8 weeks of age. n = 5 mice. Scale bar, 100 μm.

(H) Quantification of Wnt$^+$ adipocytes among total adipocytes in (G).

Data are mean ± s.e.m., ***P < 0.001, unpaired Student's t-test. See also Figure S5.

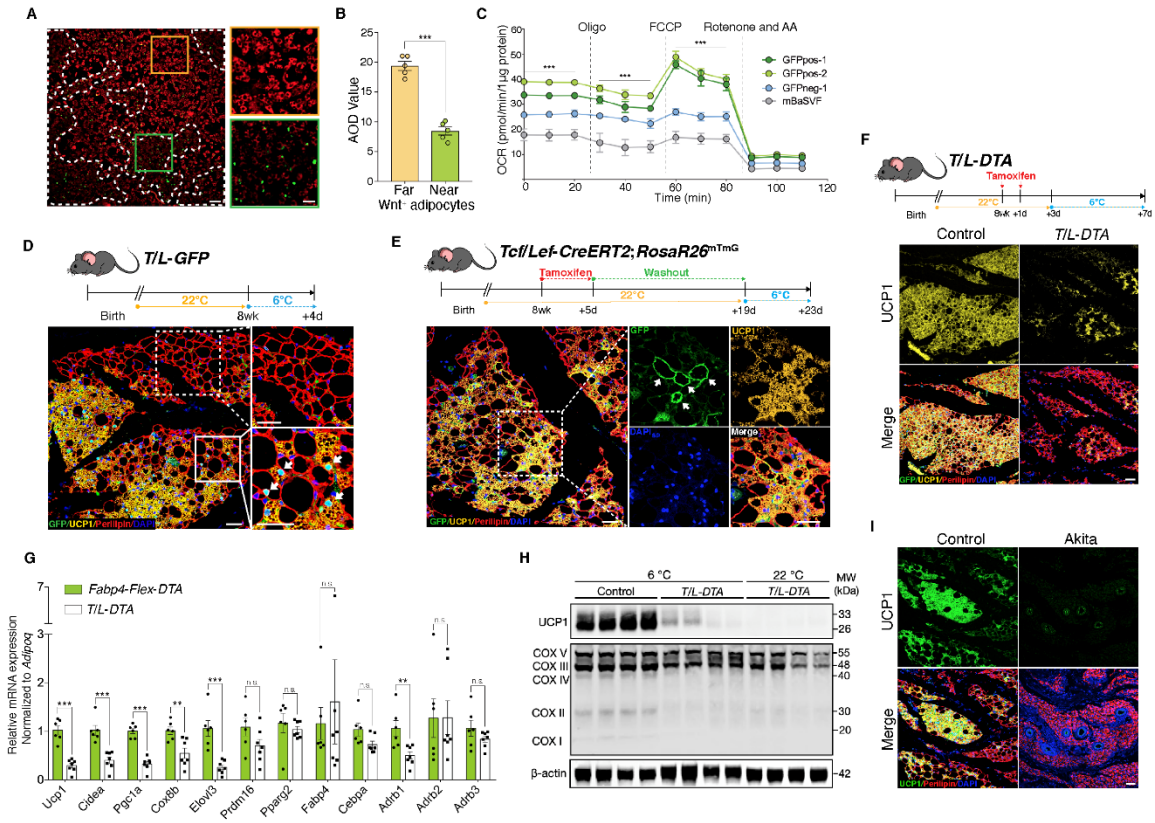

Figure 5. Wnt$^+$ adipocytes are essential for initiating adaptive thermogenesis

(A) Immunofluorescent staining of mitochondrial membrane potentials in Wnt$^+$ adipocytes induced from iBAT-derived SVF cells of *T/L-GFP* mice. $n = 5$ independent experiments. Scale bar, 100 μm; close-up scale bar, 20 μm.

(B) Quantification of staining in (A). Data are mean ± s.e.m., unpaired Student's *t*-test; ***$P < 0.001$.

(C) OCR plots of four groups of adipocytes differentiated from GFPpos-1, GFPpos-2, GFPneg-1, and mBaSVF cell lines, respectively. $n = 3$ independent experiments.

(D) Immunofluorescent staining of iWAT from *T/L-GFP* mice with 4-day thermal challenge showing close association of Wnt$^+$ adipocytes with UCP1$^+$ beige adipocytes. $n = 5$ mice. Scale bar, 100 μm.

(E) Immunofluorescent staining of iWAT from tamoxifen-treated *Tcf/Lef-CreERT2;Rosa26R*^{mTmG} mice after 4-day cold exposure. $n = 8$ mice. Scale bar, 50 μm.

(F) Immunofluorescent staining of iWAT from tamoxifen-treated *T/L-DTA* mice after 4-day cold exposure. Before cold challenge, mice were rested for 48 hours after final tamoxifen treatment. $n = 7$ mice. Scale bar, 50 μm.

(G) Quantitative RT-PCR analysis of gene expression in iWAT from control (*Fabp4-Flex-DTA*) and *T/L-DTA* mice in (F). $n = 6$ and 7 mice. Levels of mRNA expression are normalized to that of *Adipoq*.

(H) Western blot analysis showing protein levels of UCP1, OXPHOS complexes, and β-actin in iWAT from tamoxifen-treated controls and *T/L-DTA* mice under cold (6ºC) and ambient (22ºC) temperatures. $n = 4$ mice.

(I) Immunofluorescent staining for UCP1 (green) and Perilipin (red) in the iWAT from control and Akita mice. Scale bars, 50 μm.

Data are mean ± s.e.m., *$P < 0.05$, ** $P < 0.01$, ***$P < 0.001$, n.s., not significant, two-way repeated ANOVA followed by Bonferroni's test (C) or unpaired Student's *t*-test (G). See also Figure S6.

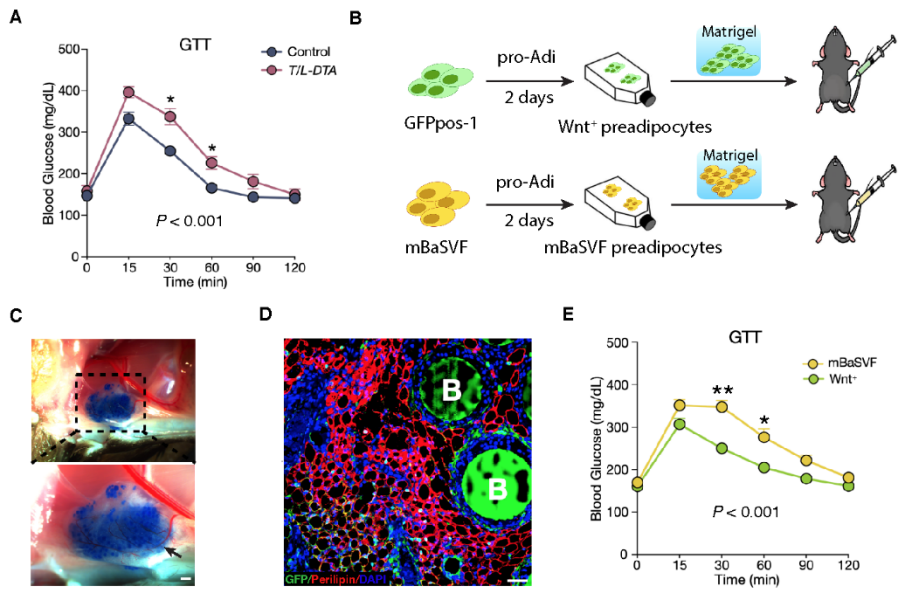

Figure 6. Wnt$^+$ adipocytes enhance systemic glucose homeostasis

(A) Glucose tolerance test (GTT) in tamoxifen-treated control (*Fabp4-Flex-DTA*) and *T/L-DTA* mice on regular chow diet. $n = 7$ mice each.

(B) Schematic of Wnt$^+$ adipocyte gain-of-function studies by cell implantation.

(C) Photographs of fat pad formed by implanted cells. Blue agarose beads were included to locate the Matrigel pad. Black arrow shows benign vascularization of fat pad within two weeks. Scale bar, 50 µm.

(D) Immunofluorescent staining for Perilipin showing mature adipocytes and accompanied agarose beads (marked by B) in the ectopically formed fat pad in (C). Scale bar, 50 µm.

(E) GTT in mice that received implantation of committed pre-adipocytes/adipocytes from mBaSVF ($n = 8$ mice) or GFPpos-1 ($n = 7$ mice) cell lines for two weeks.

Data are mean ± s.e.m., *$P < 0.05$, ** $P < 0.01$, two-way repeated ANOVA followed by Bonferroni's test.

Supplemental Figures

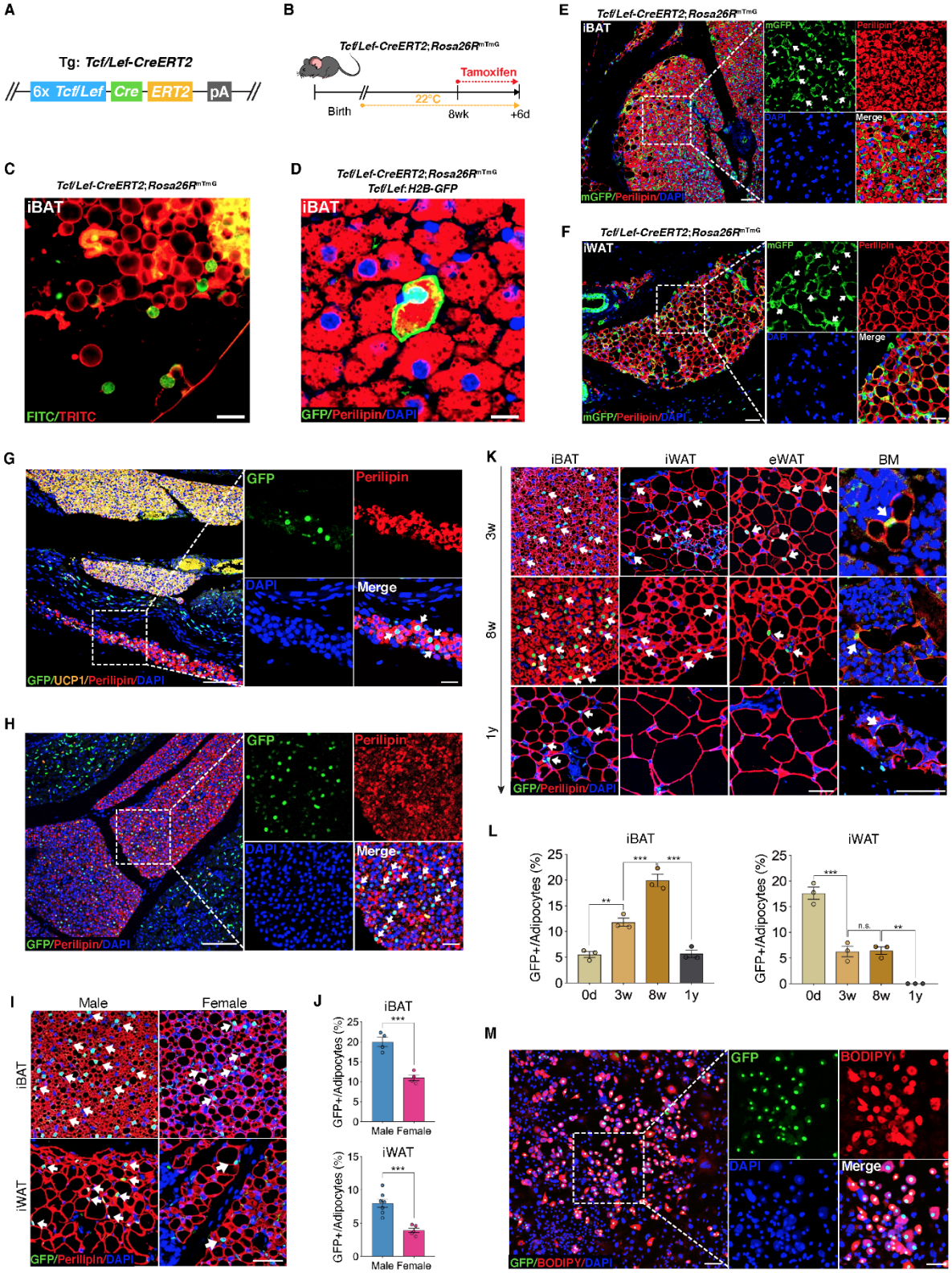

Figure S1. An inducible mouse model validates the existence of Wnt/β-catenin-positive adipocytes, related to Figure 1

(A) Schematic overview of the *TCF/Lef-CreERT2* allele.

(B) Illustration of the validation experiments in Wnt/β-catenin-positive lineage reporter mice.

(C) Microscopy images of freshly isolated mGFP-positive adipocytes from iBAT of *TCF/Lef-CreERT2*;*Rosa26R*^{mTmG} mice.

(D) GFP expression in the cell membrane and nucleus of an adipocyte in *Tcf/Lef-CreERT2*;*Rosa26R*^{mTmG};*T/L-GFP* mice. Scale bar, 10 μm.

(E and F) *Tcf/Lef-CreERT2;Rosa26R*^{mTmG} mice exhibited mGFP-positive adipocytes (white arrows) in iBAT (E) and iWAT (F) after tamoxifen treatment. $n = 4$ mice each. Scale bars, 50 μm; close-up scale bars, 20 μm.

(G) Immunofluorescent images of subcutaneous WAT adjacent to iBAT from E17.5 *T/L-GFP* mouse showing initial appearance of Wnt$^+$ adipocytes. $n = 3$ embryos. Scale bar, 100 μm; close-up scale bar, 25 μm.

(H) Immunofluorescent images of iBAT from E18.5 *T/L-GFP* mice showing initial appearance of Wnt$^+$ adipocytes. $n = 3$ embryos. Scale bar, 100 μm; close-up scale bar, 25 μm.

(I) Immunofluorescent images of iBAT and iWAT from adult male and female mice showing Wnt$^+$ adipocytes. $n = 4$-7 mice. Scale bar, 50 μm.

(J) Quantification of Wnt$^+$ adipocytes among total adipocytes in (I).

(K) Immunofluorescent images of various fat depots from *T/L-GFP* mice at different ages showing the presence of Wnt$^+$ adipocytes. $n = 3$ mice each. Scale bar, 50 μm.

(L) Quantification of Wnt$^+$ adipocytes among total adipocytes in (K).

(M) Immunofluorescent images of Wnt$^+$ adipocytes induced from E13.5 MEFs *in vitro*. $n = 2$ independent experiments from 8 embryonic mice, 3 independent wells each. Scale bar, 100 μm; close-up scale bar, 20 μm.

White arrows in all panels point to Wnt$^+$ adipocytes. Data are mean ± s.e.m., $^{**}P < 0.01$, $^{***}P < 0.001$, n.s., not significant, unpaired Student's *t*-test (J) or one-way ANOVA followed by Tukey's test (L).

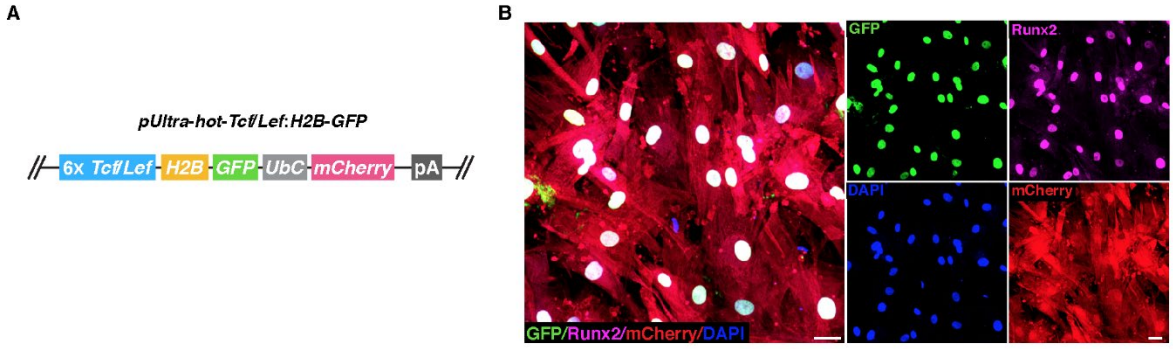

Figure S2. Infection of lentiviral virus in hBMSCs study, related to Figure 1

(A) Construct of the lentiviral shuttle vector.

(B) Representative immunofluorescent images of infected hBMSCs in pro-osteogenic differentiation medium showing the expression of GFP in the nuclei of osteocytes, indicative of the activation of Wnt/β-catenin signaling. $n = 2$ independent experiments, 3-4 independent wells each. Scale bars, 50 μm.

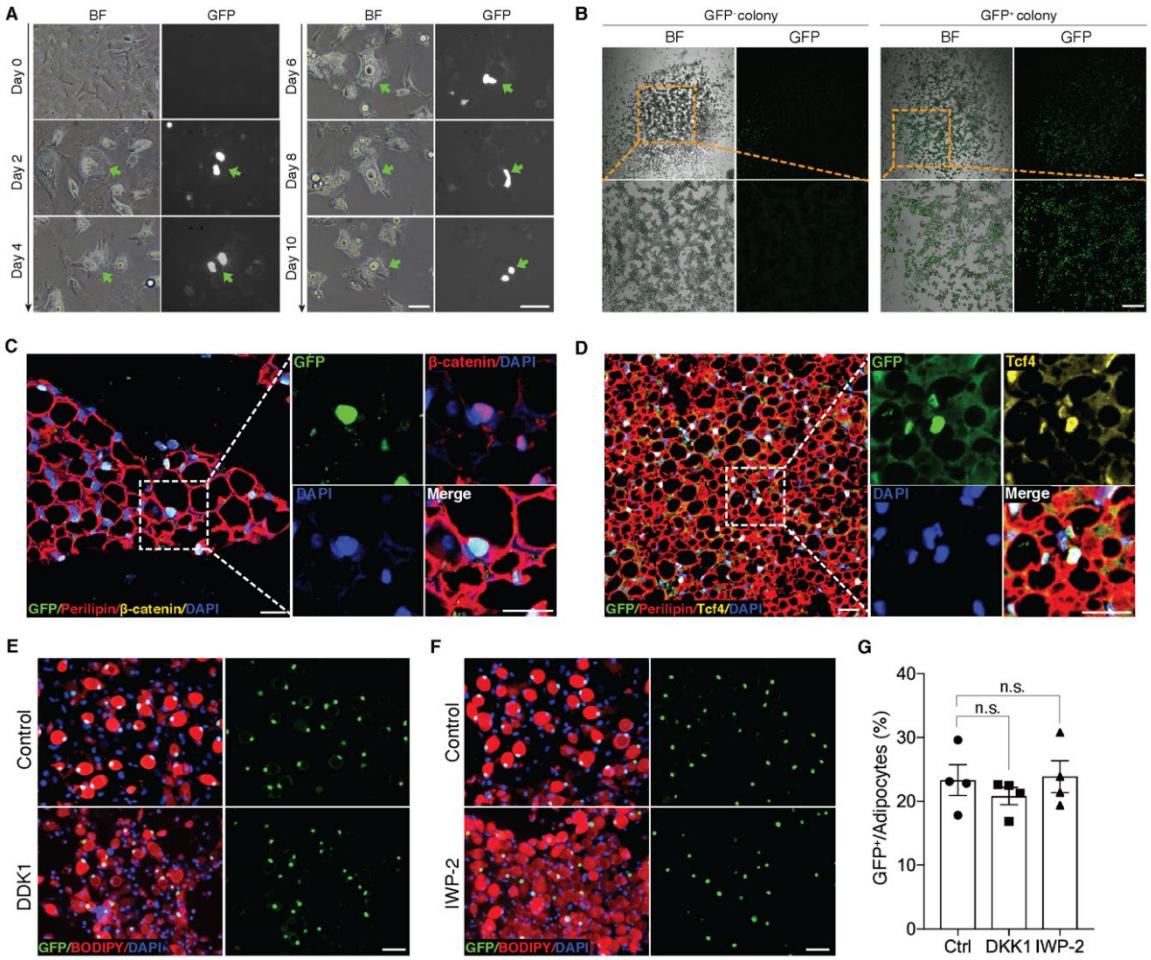

Figure S3. Intracellularly activated Wnt/β-catenin signaling that is also involved in the regulation of adipogenic maturation, related to Figure 2

(A) Microscopy images of GFP^- and GFP^+ colonized adipocytes after 7-day differentiation induced from BMSCs of *T/L-GFP* mice. $n = 4$ independent experiments. Scale bar, 200 μm.

(B and C) Immunofluorescent images of active β-catenin (B) and Tcf7l2 (C) in Wnt^+ adipocytes. $n = 3$ mice each. Scale bars, 20 μm (B), 25 μm (C).

(D and E) Immunofluorescent images of induced Wnt^+ adipocytes from BMSCs of *T/L*-GFP mice treated with DKK1 (D) and IWP-2 (E). $n = 4$ independent experiments each. Scale bars, 50 μm.

(F) Quantification of Wnt^+ adipocytes among total adipocytes in (D) and (E).

(G and H) Immunofluorescent images of Wnt^- adipocytes induced from two independent cell lines (GFPneg-1 and -2) with LF3 treatment (50 μM) for one (G) and two days (H), respectively. LF3 was added into the medium after 3-day pro-adipogenic induction. Note that by 1-day LF3 administration, Wnt^- adipocytes began to show delayed adipogenic maturation. By 2-day LF3 administration, delayed adipogenic maturation in Wnt^- adipocytes became clear, compared to controls. Scale bar, 100 μm.

(I) Microscopy images of Oil Red O staining in adipocytes induced from GFPneg-1 and -2 cell lines showing reduced lipid accumulation by LF3 treatment for two days. $n = 3$ independent experiments. Scale bar, 50 μm.

(J) Quantitative RT-PCR analysis of the expression of adipogenic genes in (I). The levels of mRNA expression are normalized to that of *36B4*.

Data are mean ± s.e.m., $^{**}P < 0.01$, $^{***}P < 0.001$, n.s., not significant, one-way ANOVA followed by Tukey's test (F) or unpaired Student's *t*-test (J).

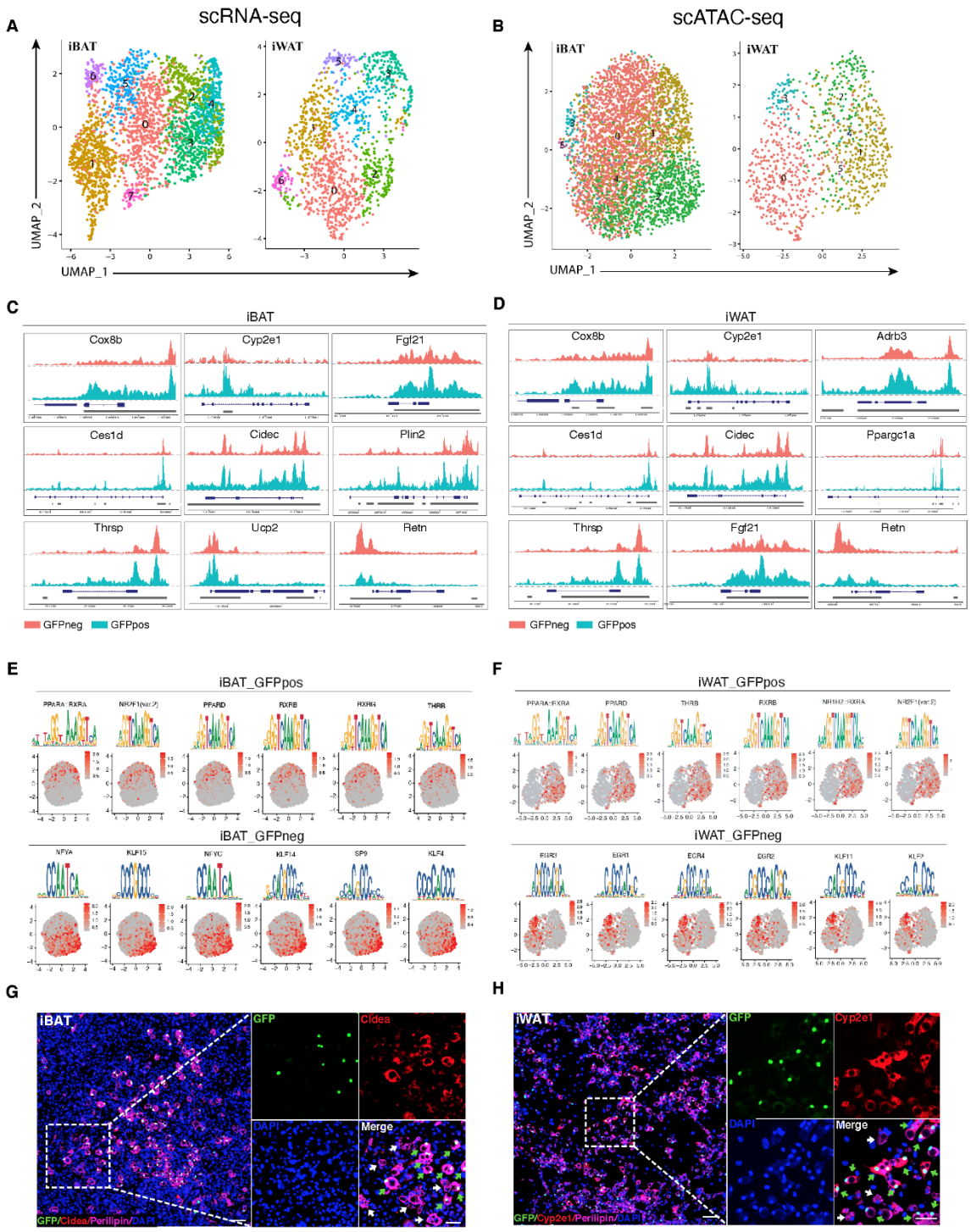

Figure S4. Wnt$^+$ adipocytes are distinct from Wnt$^-$ ones in molecular signatures, related to Figure 3

(A and B) UMAP visualization of unsupervised clustering in scRNA-seq (A) and scATAC-seq (B).

(C and D) ScATAC-seq tracks of iBAT- (C) and iWAT-derived (D) Wnt$^+$ and Wnt$^-$ adipocytes showing distinct chromatin accessibilities of representative genes.

(E and F) Enriched DNA motifs of iBAT- (E) and iWAT-derived (F) Wnt^+ (upper panels) and Wnt^- (lower panels) adipocytes in scATAC-seq.

(G and H) Immunofluorescent staining of Cidea in adipocytes induced from iBAT-derived SVFs (G) and Cyp2e1 in adipocytes induced from iWAT-derived SVFs (H). White arrows point to Wnt^- adipocytes without Cidea or Cyp2e1 expression, green arrows point to Wnt^+ adipocytes with positive staining of indicated protein. n = 3 independent experiments. Scale bars, 100 μm; close-up scale bars, 25 μm.

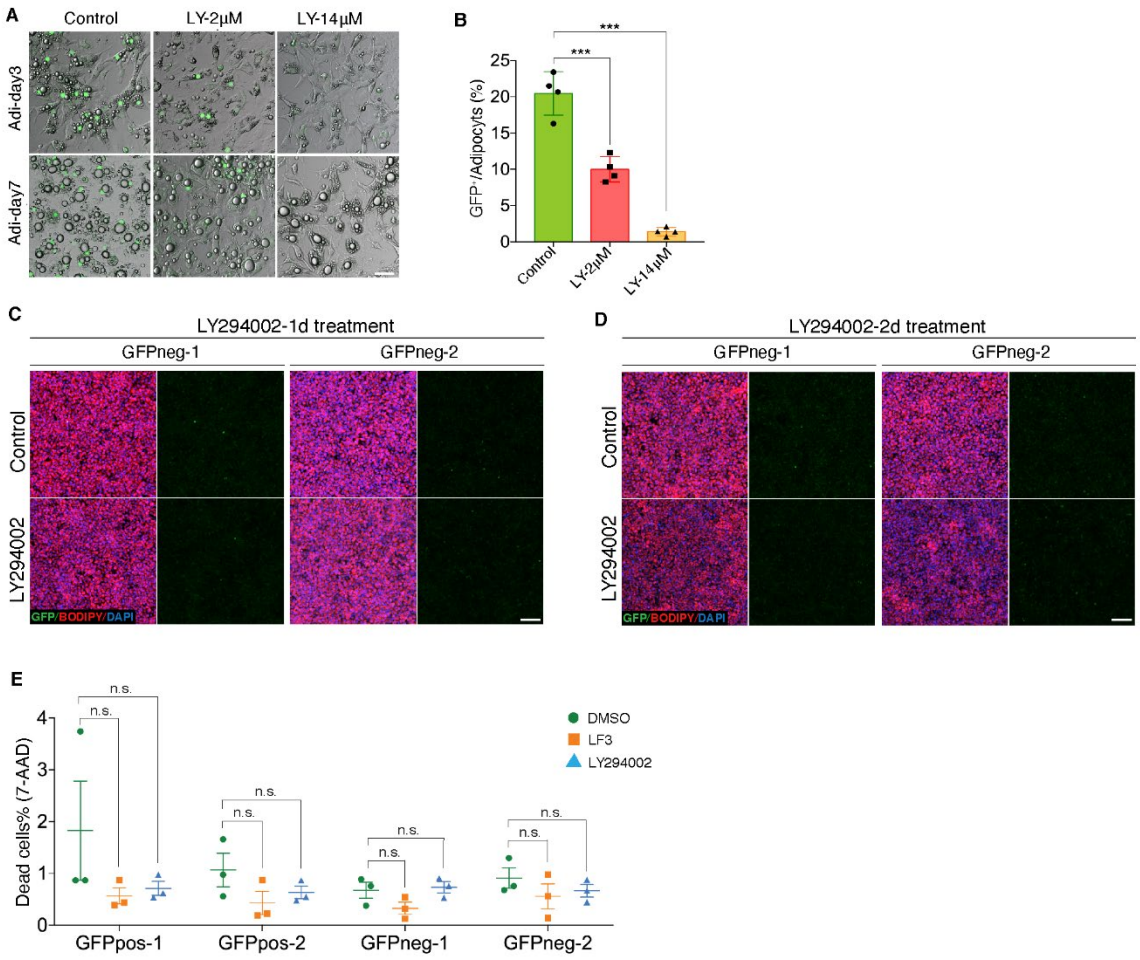

Figure S5. Inhibition of Akt signaling by LY294002 yields similar results as LF3 treatment, related to Figure 4

(A) Microscopy images of LY294002-treated adipocytes showing reduced number of Wnt^+ adipocytes and delayed adipogenesis after 3- and 7-day treatment compared to controls. $n = 4$ independent experiments. Scale bar, 20 μm.

(B) Quantification of Wnt^+ adipocyte among total adipocytes after 7-day treatment in (A).

(C and D) Immunofluorescent images of Wnt^- adipocytes induced from two independent precursor cell lines (GFPneg-1 and -2) with LY294002 treatment (14 μM) for one (C) and two days (D), respectively. LY294002 was added into the medium after 3-day pro-adipogenic induction. LY294002 treatment led to slightly reduced lipid storage in Wnt^- adipocytes. $n = 5$ independent experiments. Scale bar, 100 μm.

(E) Quantification of the percentage of 7-AAD-positive cells by flow cytometry analyses showing comparable cell viability in immortalized GFPpos and GFPneg precursor cell lines treated with LF3, LY294002, or DMSO at the same doses. $n = 3$ independent experiments.

Data are mean ± s.e.m., ***$P < 0.001$, n.s., not significant, one-way ANOVA followed by Tukey's test.

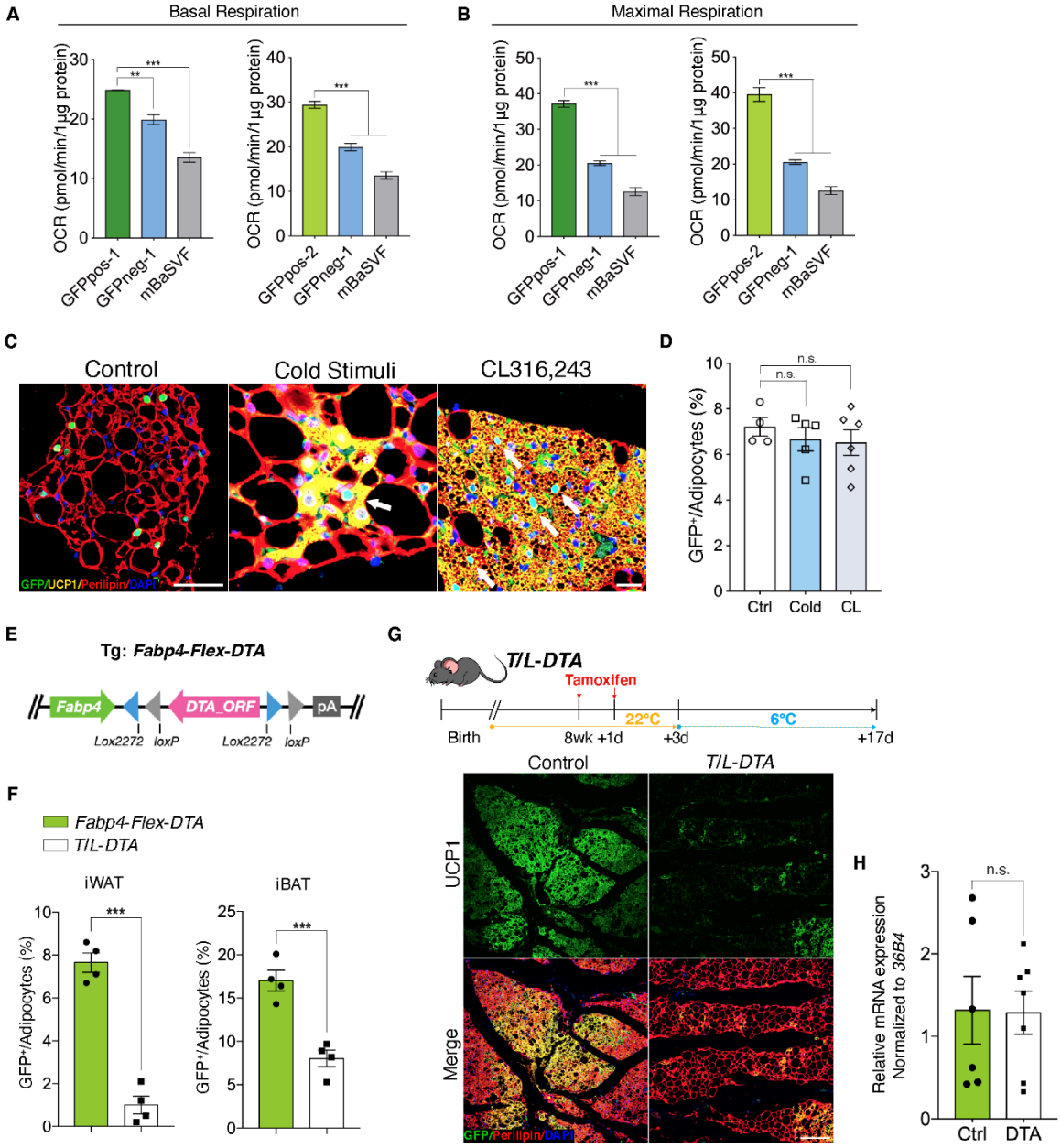

Figure S6. Wnt$^+$ adipocytes participate in adaptive thermogenesis in iWAT, related to Figure 5

(A and B) Calculated basal (A) and maximal (B) respiration levels in OCR assay in **Figure 5C**.

(C) Immunofluorescent images of iWAT from *T/L-GFP* mice after 2-day cold stress (n = 5 mice), CL316,243 treatment (n = 6 mice), and control (n = 4 mice). Scale bar, 100 µm.

(D) Quantification of Wnt$^+$ adipocytes among total adipocytes in (C).

(E) Schematic overview of the *Fabp4-Flex-DTA* allele.

(F) Quantification of Wnt^+ adipocytes among total adipocytes of iWAT and iBAT from *Fabp4-Flex-DTA*;*T/L-GFP* and *T/L-DTA*;*T/L-GFP* mice 24 hours after 2-day tamoxifen treatment prior to cold challenge. $n = 4$ mice each.

(G) Immunofluorescent staining of iWAT from tamoxifen-treated *T/L-DTA* mice after 2-week cold exposure. Before cold challenge, mice were rested for 48 hours after the second tamoxifen injection. $n = 4$ mice. Scale bar, 50 μm.

(H) Quantitative RT-PCR analysis of *Adipoq* expression in iWAT from control (*Fabp4-Flex-DTA*) and *T/L-DTA* mice in **Figure 5G**, showing comparable results between two groups. $n =$ 6 and 7 mice. The levels of mRNA expression are normalized to that of *36B4.*

Data are mean ± s.e.m., $^{**}P < 0.01$; $^{***}P < 0.001$, one-way ANOVA followed by Tukey's test (A, B, and D) or unpaired Student's *t*-test (F and H).